Electrochemical properties of MnO₂-based carbon nanomaterials for energy storage and electrochemical sensing

Emtinan Ouda[1,*], Nehad Yousf[1,*] , Hend S. Magar[2], Rabeay Y. A. Hassan[3], and El-Shazly M. Duraia[1]

[1] *Physics Department, Faculty of Science, Suez Canal University, Ismailia 41522, Egypt*

[2] *Applied Organic Chemistry Department, National Research Centre (NRC), Dokki 12622, Giza, Egypt*

[3] *Nanoscience Program, University of Science and Technology (UST), Zewail City of Science and Technology, Giza 12578, Egypt*

ABSTRACT

Electrochemical alongside the electro-catalytic properties of graphene and multi-walled carbon nanotubes have been improved via doping with manganese oxide nanostructures. Structural, morphological, and electrochemical properties of the as-synthesized nanocomposites were identified using XRD, FTIR, SEM, and electrochemical methods including cyclic voltammetry, and electrochemical impedance spectroscopy. The SEM images showed flower-like microsphere structures, while the conjugation of MnO_2 with the carbon nanomaterials was confirmed by the FTIR and XRD analysis. All MnO_2-based nanocomposites provided great enhancement in their electrochemical activities with a larger value of specific capacitance than the individual constituents of carbon nanomaterials. Accordingly, hydrogen peroxide-directed detection was evaluated, whereas the nanocomposites exhibited direct electron transfer, fast and linear responses in the range from 1.0 to 210 μM. Thus, the significant enhancements in the electrochemical features acquired by the nanocomposites could suggest these nanomaterials for energy storage and hydrogen peroxide sensing applications.

1 Introduction

Numerous efforts have been made in recent years to create better energy storage technologies aiming to solve the increasing clean energy demand under the rising environmental and climate change. Supercapacitors, also known as electrochemical capacitors, have been viewed as one type of promising energy storage technology due to their high-power density, long lifetime, and very fast charge/discharge rates [1, 2]. High efficient energy storage systems and consumer electronic devices is

Address correspondence to E-mail: emtnan_oda@science.suez.edu.eg; Nehad_yousf@science.suez.edu.eg

Springer

highly desired because of the global energy problem arising from the increasing population and international economic growth.

In principle, RuO_2, NiO, Co_3O_4, and MnO_2 are well-known transition metal oxides (TMOs) that have been widely studied as supercapacitor electrode materials [3–6]. The fact that they store energy through fast, reversible redox reactions, which are called pseudo-capacitance. Among TMOs manganese dioxide (MnO_2) is one of the most significant materials for supercapacitors due to its superior specific capacitance [7, 8], not harmful to the environment, and lower cost [9]. However, due to the insufficient electronic conductivity of MnO_2 as well as its relatively lower specific surface area, the electrochemical efficiency of MnO_2 is limited. [10]. MnO_2 on the nanoscale can offer a significantly greater surface area, increasing storage capacity and enhancing specific capacitance.

However, it has been found that pure MnO_2 nanostructures are easily destroyed during the redox process, which lowers the cycle stability [11]. During reaction in a supercapacitor, micro-cracks occur, and the volume expansion happens for the electrode materials. To solve this situation, intensive work has focused on new nanoscale materials. For example, activated carbon, carbon nanotubes, and fullerene-C_{60} graphene were conjugated with the MnO_2 to improve the electrochemical efficiency, and the electro-catalytic properties [12–15].

Currently, carbon nanomaterials CNMs are the most studied material for energy storage electrode in pseudo-capacitor, electric double layer capacitor (EDLC), and Li-ion battery [16–19]. The results demonstrated the high potential of carbon-based materials to improve today's energy storage field. Specifically, they could enhance several features for energy storage devices. e.g., flexible and smaller capacitors, [20], transparent batteries, with high capacity and fast charging ability.

Nevertheless, CNMs have low volumetric energy density and low specific capacitance [21, 22]. Thus, the CNMs-based metal oxide nanocomposites are suggested to overcome this problem. In this regard, there is a challenge to prepare CNMs/TMOs composite with simple and low-cost preparation methods with good electrochemical properties.

On the other hand, synthesis of nanomaterials with the aid of microwave irradiation has many advantages such as fast, easy, symmetric, and energy-efficient heating. Consequently, the microwave-assisted approaches have been widely applied to synthesize such nanomaterials [23], inorganic complexes, nanocrystalline particles, and organic compounds. In contrast to pristine carbon, microwave irradiation plays an effective role to activate the surface pores of carbon and significantly raises specific capacitance. A few articles have been studying the synthesis of GO/CNTs/MnO_2 composites prepared by microwave assistants. Zhang et al. prepared RGO/MnO_2-CNTs by microwave-assisted hydrothermal and the specific capacitance value reached 250 F g^{-1} at $10Ag^{-1}$ in 1.0 M of Na_2SO_4 as an electrolyte [24]. On the other hand, CNMs-based metal oxides have been intensively studied as a promising material for improving the performance and efficiency of sensors [6], 25, 26. For instance, the detection of hydrogen peroxide has received great attention due to its significance in a number of industrial sectors [6].

Here, microwave-assisted synthesis was utilized for the fast fabrication of MnO_2-based nanocomposites, without any further preparation process like the other chemical synthesis methods. The structure and morphological characterization of all nanocomposites have been identified in order to identify all chemical and physical characters. The newly synthesized nanocomposites exhibited good enhancement in their electrochemical properties including high electrical conductivity and high catalytic activity. For this reason, the sensing behavior of the as-synthesized materials was evaluated for the direct amperometric detection of hydrogen peroxide.

2 Experimental work

2.1 Materials and methods of characterization

Multiwall carbon nanotubes (MCNTs) powder was obtained from Nanoridge-Houston-USA. Potassium permanganate, sulfuric acid and manganese chloride hexahydrate from loba-chemie PVT-LTD in India. X-ray diffraction (XRD) analyses were performed using Philips (Model X-Pert). FTIR spectroscopic analysis was performed using the Nicolet 6700 FTIR spectrometer within the range of 400–4000 cm^{-1}. The surface morphology of nanocomposites was morphology using a scanning electron microscope (SEM Model Quanta-250 FEG). Electrochemical studies

were carried out using screen-printed electrodes (SPEs) which contain three-electrode system (working, counter and reference electrodes). Palmsens-4-potentiostat electrochemical workstation.

2.2 Synthesis of carbon nanomaterials

Graphene oxide (GO) was chemically synthesized using the modified Hummers protocols [27, 28]. In detail, 1.0 g of graphite powder and 0.5 g sodium nitrate with 23 ml sulfuric acid were mixed in 500 ml flask put it in an ice bath. Afterward, 3.0 g potassium permanganate was slowly added, followed by stirring for 2 h. After that, the flask was transferred to a water bath at 35 °C and the mixture was stirred for another 30 min. A 46 ml of deionized (DI) water was added, the temperature was raised to 98 °C. The mixture was maintained at this temperature for 30 min. Then, additional 140 ml of DI water and 10 ml of hydrogen peroxide (H_2O_2) were added sequentially. The product was filtered and washed with 5% HCl. Followed by washing with DI water several times and finally drying at 60 °C to obtain GO powder.

For MCNTs preparation, CNTs were modified by microwave-assisted route before being used. Briefly, the solution of (1.0 mg/ml) CNTs was stirred for 5 min with a small droplet of surfactant. Afterward, CNTs solution was exposed to microwave radiation for 5.0 min with moderate power. The final MCNTs powder was obtained after drying at 60 °C.

2.3 Synthesis of MnO_2/GO and MnO_2/MCNTs nanocomposites

The previously published microwave-assisted synthesis approaches were applied [27], whereas the MnO_2 nanoparticles were prepared firstly. Briefly, 0.3 g potassium permanganate was slowly added to $MnCl_2.6H_2O$ solution (10 mg/ml) under continuous stirring for 20 min. The mixture was exposed to microwave irradiation for 5.0 min, and then it was washed, filtered out, and dried to obtain the MnO_2. By following the same steps, MnO_2/GO and MnO_2/MCNTs nanocomposites were prepared, whereas 50 ml of GO suspension (1.0 mg/ml) or MCNTs (1.0 mg/ml) was added. To obtain the MCNTs/MnO_2/GO, 0.5 g of $MnCl_2.6H_2O$, in addition to 25 ml of each suspension of (1.0 mg/ml) CNT, and (1.0 mg/ml) GO were mixed and stirred for 30 min.

Next, a 0.3 g of potassium permanganate was added gradually with stirring for 20 min. The resultant mixture suspension was further irradiated with a microwave for 5 min, filtered out and dried at 60 °C to obtain the MCNTs/MnO_2/GO nanocomposite. Scheme 1 illustrates the preparation steps of the nanocomposites.

## 2.4 Electrochemical characterization and electrode modification

For the modification of working electrodes (sensor chips) with the nanomaterials, 5.0 mg of the synthetic nanocomposite was suspended in 1.0 ml of double distilled water, and then ultrasonicated for 30 min to produce a homogenous suspended solution. A 30 μl of the suspended solution was drop-casted on the electrode surface and left to dry at room temperature. For SPE characterization, CV and EIS measurements were conducted in 5.0 mM of ferricyanide [Fe $(CN)_6]^{3-/4-}$, as the standard redox probe in 0.1 M KCl (as the supporting electrolyte). Scheme 2 summarizes the fabrication and electrochemical characterization steps.

3 Results and discussion

3.1 XRD analysis

Crystalline and structural features of the as-synthesized nanomaterials were investigated using the XRD, as shown in in Fig. 1. For the GO sample, an intense peak at $2\theta = 10.5°$ has been observed which is corresponding to shifted plan (002) of GO due to the functional groups intercalated between the sheets with an interplanar distance of d = 0.8 nm. One more less-intensive peak was obtained at $2\theta = 26.2°$ with interplanar distance of = 0.34 nm to refer to the unaffected (not oxidized) graphite layers. The significant shift of two theta towards the lower values indicated the increase in d-spacing, which is considered as an evidence to the intercalation of functional groups and the successful formation of GO. These characteristic peaks of GO have good agreement with previously published reports [29–31]. On the other hand, in the case of CNTs, XRD peaks were slightly broadened. Two significant characteristic peaks were

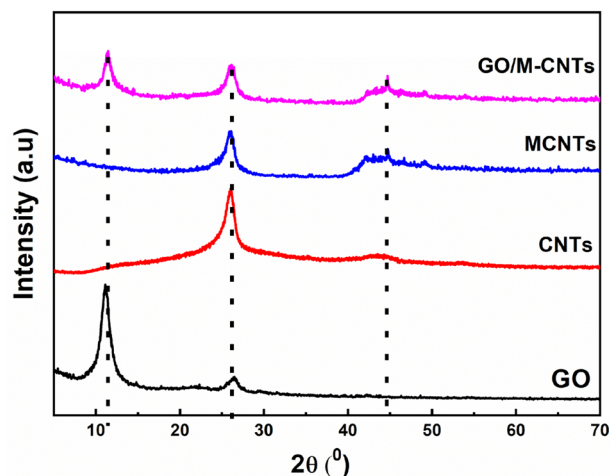**Scheme 1** Schematic illustration of the preparation procedure of the different nanocomposites
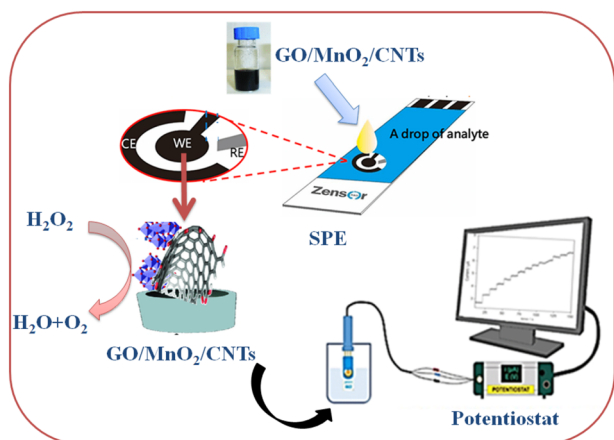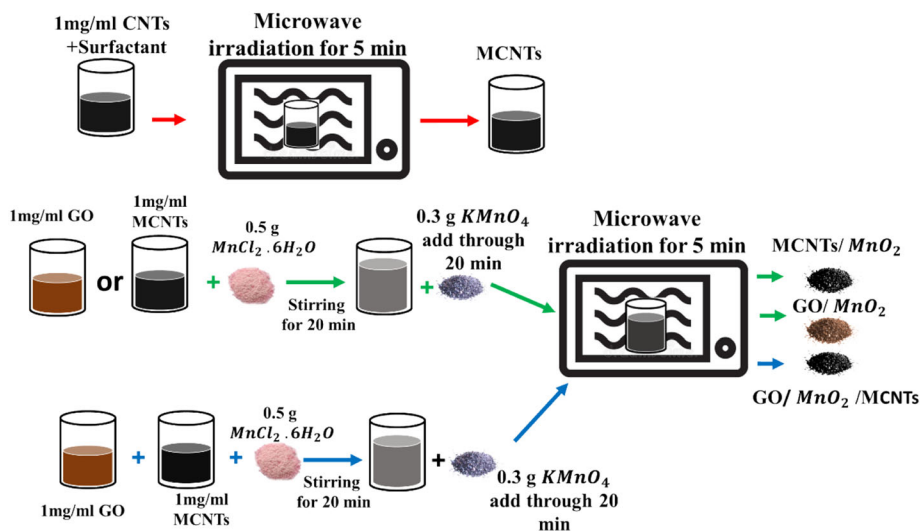
Scheme 2 Steps of SPEs modification with the prepared nanocomposite before testing their electrochemical properties using a portable potentiostat
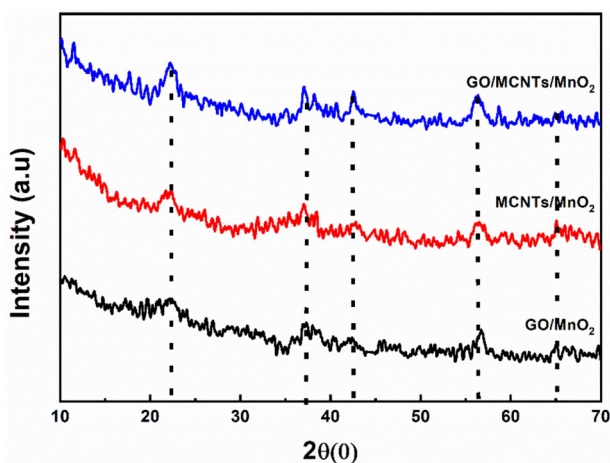

Fig. 1 XRD analysis of GO, CNTs, MCNTs, and GO/MCNTs samples

obtained at 26.2° and 44.8° which are related to (002), and (100) planes of graphite [30, 31]. The composite of MCNTs and GO displayed the typical peaks of both constituents (GO and MCNTs) reflecting the successful dispersion of the GO among the CNTs.

On the other hand, interspacing layer was calculated by Bragg's equation ($n\lambda = 2d\sin\theta$) where n is an integer, λ is the wavelength of the diffracted x-ray, d is the spacing of the crystal layers, and θ peak position [32].

The XRD of carbon nanomaterials doped by MnO_2 shown broaden peaks at 2θ around 22°, 37°, 42 and 56° (Fig. 2) for all nanocomposites, the pattern indexed to the pure orthorhombic gamma-phase of MnO_2 consistent with the (JCPDS) 14-0644 [33, 34]. However, the characteristic peaks of CNTs and GO
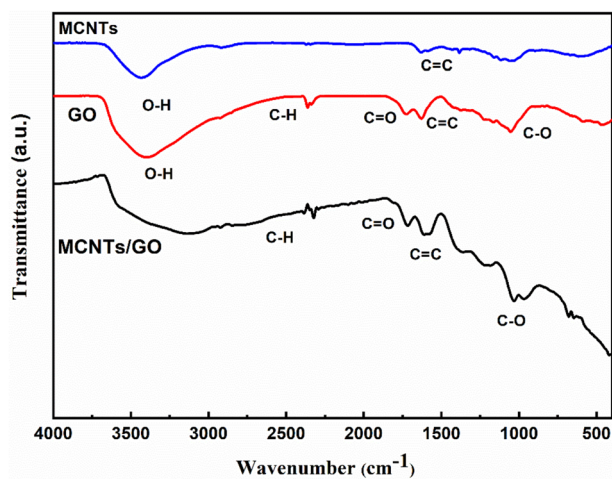

Fig. 2 XRD of prepared nanocomposites of MnO_2 doped with different carbon nanomaterials

from Fig. 1 were not observed in the MCNTs/MnO$_2$, GO/MnO$_2$ and GO/MCNTs/MnO$_2$ nanocomposites. The most likely cause is due to the formation of the thick coating layer of the MnO$_2$ coated the nanocomposite while the presence of carbon nanomaterials confirmed in the subsequent structure analysis.

3.2 FTIR analysis

FTIR analysis is very crucial to identify chemical functional groups, and the formed intermolecular forces among the formation of hybrid or mixture from different compounds. Thus, the FTIR was applied here. As illustrated in Fig. 3, the most intensive and remarkable peaks of GO were found at wavenumber 3400 cm^{-1} that is related to O–H stretching vibrations of the adsorbed water molecules and the peak at 1720 cm^{-1} is attributed to the C=O stretching vibration from carbonyl and carboxyl groups. These resultant peaks indicated the attachment of the oxygen-containing functional groups to the carbon skeleton of graphite during the oxidation process to form the GO. The adsorption peak at 1600 cm^{-1} is assigned to the components from the un-oxidized graphitic domains (C=C). The MCNTs spectra showed the aromatic C=C at around 1600 cm^{-1} (the characteristic band of all carbon nanomaterials) beside some functional groups such as the O–H (3500 cm^{-1}), and C–O (1030 cm^{-1}) due to the pretreatment of the pristine CNTs. A combination of the characteristic FTIR peaks of GO and MCNTs

were collected in Fig. 3 for the GO/MCNTs composite.

On the other hand, the FTIR results of the MnO$_2$ nanocomposites (depicted in Fig. 4) showed a distinctive peak around 430 cm^{-1} this peak is attributed to MnO$_2$ vibrational mode [35, 36]. Similar peaks for all samples have been appeared at the same positions indicating the successful formation of the nanocomposites that contain carbon nanomaterials combined with the MnO$_2$. Other less-intensive peaks that are related to carbon nanomaterials were obtained as illustrated in the previous section for FTIR results of GO, MCNTs, GO/MCNTs.

3.3 Morphological analysis

SEM images were used to show the microscopic surface morphology of the prepared nanomaterials, as shown in Fig. 5. Graphene oxide nano-sheets appeared in Fig. 5A indicating the successful exfoliation process. Smooth carbon nanotubes with diameter around 80 nm and few micrometers in length were clearly shown in Fig. 5B, whereas the smoothen of CNTs changed to quiet roughness due to the treatment with the surfactant in MCNTs sample (Fig. 5C). It is worth mentioning that no change in diameter or length was observed. From Fig. 5D, MCNTs with large area nano-sheets of GO together in GO/MCNTs nanocomposites were obtained.

MnO$_2$ sample showed self-assembled nano-sheets to form flower-like architecture microspheres with

**Fig. 3** FTIR of carbon nanomaterials
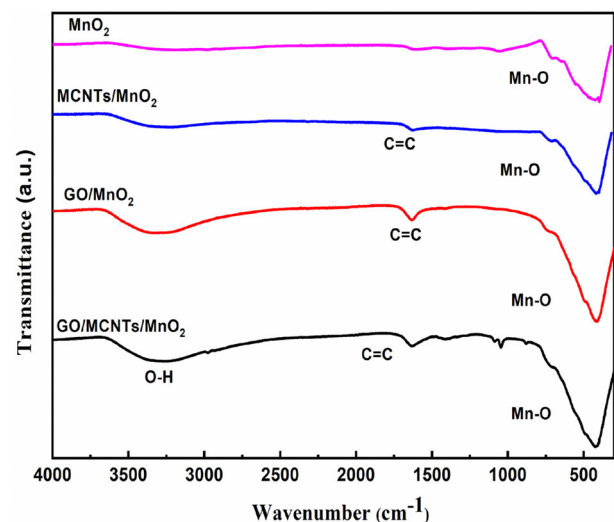
Fig. 4 FTIR of the prepared nanocomposites (MnO$_2$-based carbon nanocomposites)
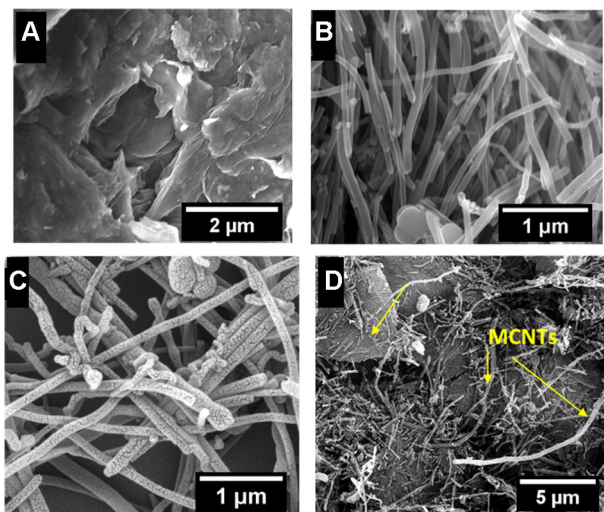
Fig. 5 SEM image of **A** GO, **B** CNTs as received, **C** MCNTs after microwave irradiation treatment **D** GO/MCNTs nanocomposites

sphere diameter in the range of 200–300 nm (Fig. 6a). Further, 3D images of the SEM revealed that these microspheres are composed of interconnected well-defined ultrathin nano-flakes, which form a network of flower-like nanostructures. The sphere structure of MnO_2 nanomaterials exhibited a high spongy cluster structure referring to the high specific surface area, and increasing the rate capacity and cycling stability of the MnO_2 materials. MnO_2 clearly appeared on graphene oxide sheets in Fig. 6b for GO/MnO_2 - nanocomposite while in Fig. 8c the MCNTs and MnO_2 nano-spheres were distinguished in the whole MCNTs/MnO_2 materials.   Almost   the   same
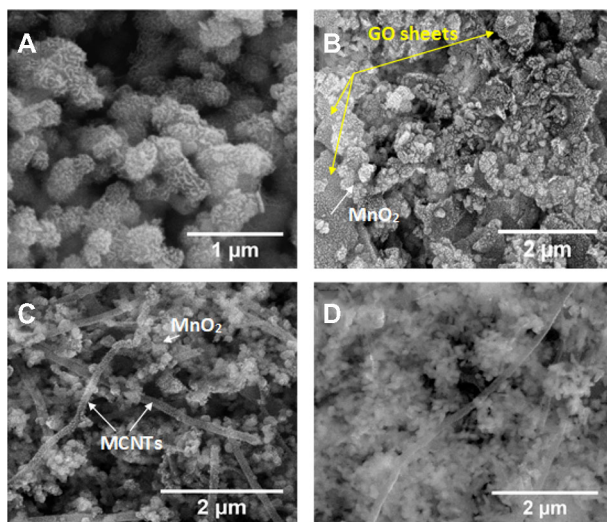
Fig. 6 SEM images of **a** MnO_2, **b** GO/MnO_2, **c** MCNTs/MnO_2 and **d** GO/MCNTs/MnO_2
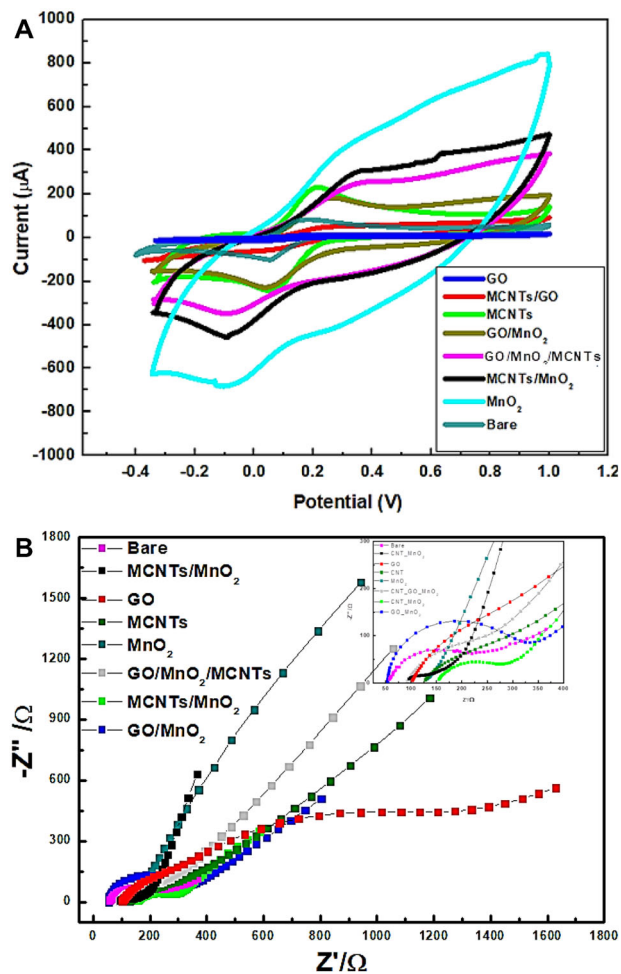
Fig. 7 A Voltammetric analysis for the nanomaterial performance. The CV measurements were conducted in a solution of standard redox probe of ferricyanide with the 5 mM in KCl as the supporting electrolyte. Scan rate of 50 mV s^{-1} was applied for all experiments. **B** EIS Nyquist spectra of modified electrodes with the nanomaterials. The inset figure represents magnification of figure B

morphology appeared for GO/MCNTs/MnO_2 - nanocomposite with faint transparent GO sheets as shown in Fig. 6d.

3.4 Electrochemical characterization of nanomaterials

In general, the storage of the electrical charge in the surface and solid phases of electrodes depends on double layer charging, faradaic processes, or a combination of both storage mechanisms. For instance, the mechanism of charging-discharging process in activated carbon electrodes is due to the charge adsorption or accumulation at the interface between

Table 1 The electrochemical parameters (CV & EIS) obtained for the modified electrodes with the prepared nanomaterials

| Electrode type	I_a (µA)	I_c (µA)	$E_{oxd.}$ (V)	$E_{red.}$ (V)	ΔE_p (V)	ΔE (V)	R_s (Ω)	$R_{ct\,(1)}$ (Ω)	W (Ω)	SC (F/g)
Bare	73.1	− 99.6	0.18	0.054	0.126	0.12	55.6	225.6	187.5	
GO	8.3	− 12.76	0.22	0.029	0.195	0.126	102	1320.2	325.7	8.7
MCNTs	200	− 221	0.21	0.056	0.159	0.135	125	130.5	115.2	158.5
MCNTs/GO	21	− 34.8	0.28	0.07	0.214	0.177	50.8	350	48.3	207.8
GO/MnO$_2$	135	− 149	0.26	0.037	0.223	0.148	150	160.4	135.2	166.5
MCNTs/GO/MnO$_2$	76.8	− 76.7	0.33	0.09	0.246	0.213	95.2	118.5	114.2	290
MnO$_2$	342	− 275	0.34	− 0.08	0.42	0.134	125	45.2	84.5	617.8
MCNTs/MnO$_2$	287	− 259	0.35	− 0.08	0.34	0.0054	90	65.8	102.3	358

Those values are extracted from the above-discussed voltammetric as well as the impedimetric experiments

Table 2 Comparison of electrochemical response between GO/MnO$_2$/CNTs composite via different preparation techniques

Nanocomposites	Electrochemical performance SC: specific capacitance (F/g)	Sensor performance DL: Detection imit (µM) LR: Linear range (µM)	Synthesis method	Ref
Gr/MnO$_2$/CNTs	245 F/g (0.5A g^{-1})		Hydrothermal method	[37]
MnO$_2$/ RGO/ coated CNTs	193 F/g (0.2 A g^{-1})		Multi chemical reaction process	[38]
MnO$_2$/GNS/ CNTs	132 F/g (5 mV s^{-1})		Chemical method	[39]
Gr/MnO$_2$	188 and 130 F/g (0.25 and 4 Ag^{-1})		Electrostatic co-precipitation	[27]
CNT/MnO$_2$/GO	473 F/g (5 mV/s)		anodic aluminum oxide template method following co-filtration with GO	[40]
Gr/MnO$_2$/CNTs film	372 F/g		Complex chemical preparation steps	[24]
MnO$_2$/GR/CNT	330.75 F/g (200 mV/s)		Two chemical step approach	[40]
MnO$_2$/Gr/CNT	367 F g^{-1} (20 mV s^{-1})		Chemical-wet route	[41]
Pt/rGO-CNT paper electrode		LR:0.1–25 µM DL:0.01 µM	Sputter deposition method	[26]
Co$_3$O$_4$-rGO		LR: 15-675 µM DL:2.4 µM	Hydrothermal procedure	[42]
MnCo$_2$O$_3$/ CNTs/SPE		LR:0.1–180 µM DL:0.1 µM	Chemical preparation steps	[6]
GO/MnO$_2$/ CNTs	290 F g^{-1} (50 mV/s)	LR:1- 210 µM DL: 0.08 µM	Facile Microwave assistant	In this study

the electrode and the electrolyte, leading to the electric double layer (EDL) capacitance. This process is mostly electrostatic and non-faradaic. This indicates that there was no electron transfer across the electrode/electrolyte interface and that no chemical changes occurred inside the electrode's solid phase during the storage of electric charge. For the charge storage in a faradaic process, it is generally agreed that significant pseudo-capacitance results from the electro-sorption of ions along with surface redox
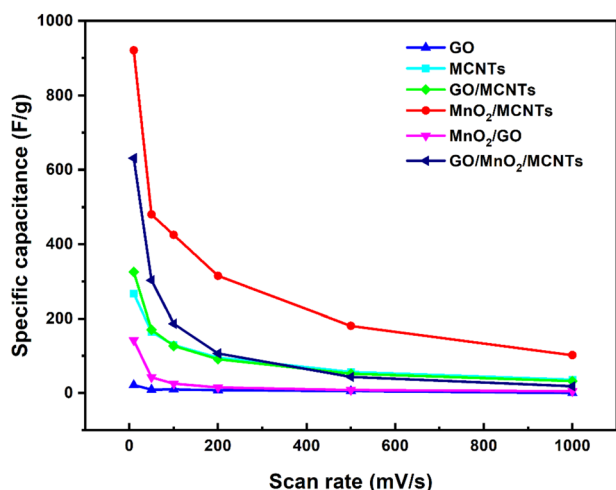
Fig. 8 Specific capacitance of all nanocomposites at different scan rates

reactions where electron transfer happens across the interface of the current collector and active material. However, it is important to note that both EDL and pseudocapacitive storage processes are capacitive. It is acknowledged that charge storage is a non-capacitive faradaic process [34]. The specific capacitance could be given using the following equation [33]:

$$C = \frac{\int I\,dV}{2 \times v \times m \times \Delta V}, \tag{1}$$

where C is the specific capacitance (F g^{-1}), v is the scan rate (V s^{-1}), m is the mass of the active material (g), ΔV is the potential difference (V), and IdV represents the area under the voltammetric peak (Q).

Consequently, the electrochemical behaviors of the prepared nanocomposites are characterized by cyclic voltammetry (CV) and electrochemical impedance spectroscopy (EIS) in a solution of the stranded redox mediator (ferricyanide). As a result, voltammetric analysis of the fabricated nanomaterials was illustrated in Fig. 7. A higher faradaic current (due to the faster oxidation–reduction of the standard redox probe) was applied for all electrodes that were modified with the nanocomposite. As reported in many researches before the untreated CNTs has a quasi-rectangular voltammogram like a supercapacitor [34, 35] while the metal oxides-based CNTs have a couple of weak oxidation/reduction peaks at 0.25 V and 0.038 V, which can be attributed to the surface functional group after treatment. The potential peak separation (ΔE_p) refers to the conductivity of materials, the larger the (ΔE_p) the less the electrode

conductivity [36]. The electrochemical parameters (CV & EIS) for all nanocomposites were shown in Table 1.

GO displayed two oxidation/reduction peaks at 0.25 V and 0.038 V, while less area under the curve was obtained to demonstrate the small specific capacitance with lower conductivity (larger ΔE_p). Due to the high electric conductivity of CNTs, they can offer a direct conductive path for MnO_2. Thus, reducing the internal resistance within the nanocomposite itself. Additionally, the CNTs inter-tube pores facilitated the fast transport of the redox species to the surface of MnO_2 from the bulk solution.

Through Fig. 7B (the Nyquist plots), semicircle portions at high frequency were shown to represent the rate of electron transfer process, whereas the diameter of the semicircle refers to the charge transfer resistance (R_{ct}) of the probe at the electrode interface. For EDLC devices, the charge transfer resistance is assumed to be the sum of the electrolyte resistance in the electrode with porous structure, the resistance of the electrode, and the contact resistance between the current collector diameter and the electrode. The presence of non-vertical line at intermediate frequencies is due to the ion transport limitation in the electrolyte in porous electrode structures. However, upon the introduction of rGO to MnO_2/CNTs, the semicircle diameter becomes smaller, indicating a higher interfacial electron transfer efficiency. These results demonstrated that the GO/MnO_2/CNTs represented an interesting electrode surface for electrochemical applications, where rGO can work as the conducting material and CNTs between rGO layers further facilitate charge transfer.

The redox peaks shown in the CV curves for the modified electrode surfaces with the nanomaterials demonstrated the significant pseudocapacitive features. In the charge/discharge process, a very fast reversible faradaic redox occurred along with the faradaic charge transfer and intercalation of protons at the surface of the electrodes.

For the GO/MnO_2/CNTs, there was no peak within the potential range of -0.38 to 1 V. This is assigned to electrical double layer-type behavior, and a non-Faradaic constant current has appeared in the entire potential range for GO/MnO_2/CNTs electrodes. However, the cyclic voltammogram exhibited a well-known hysteresis-type loop that is significant for a supercapacitor. A comparison of the specific capacity of GO/MnO_2/MCNTs electrode with
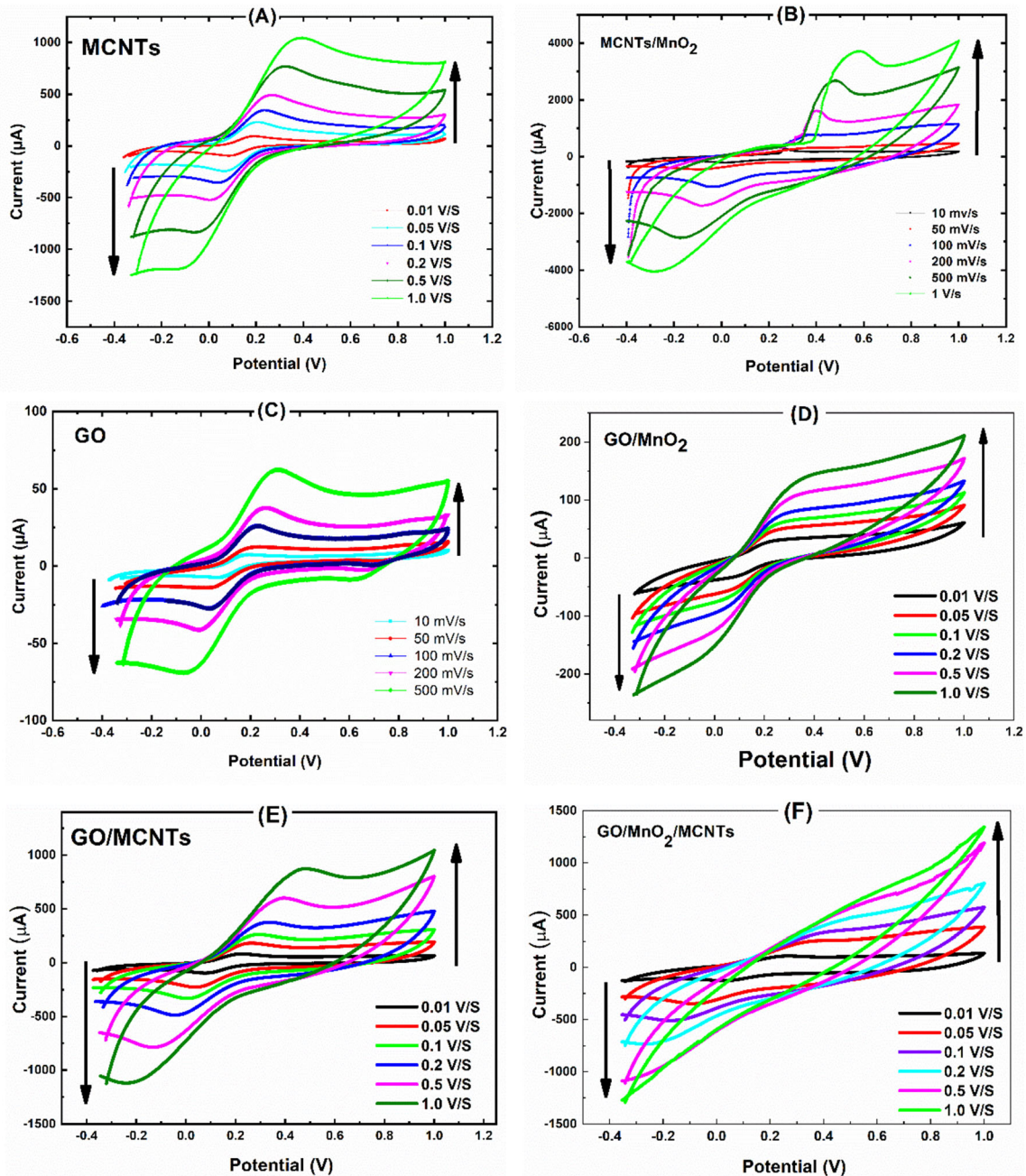
Fig. 9 CV of prepared nanocomposites at different scan rates. Screen printed electrodes were modified with a thin film of the nanomaterials and voltammetric

recently reported MnO_2 materials is shown in Table 2.

The effect of scan rate on the electrochemical performance of each prepared sample was further investigated by CV (Fig. 8). In the scan rate range from 0.1 to 1.0 V/s, a pair of symmetric redox peaks appeared, and the redox peak currents (i_{pa} and i_{pc})

were increased gradually with the increase of the scan rate.

For the GO, lower peak current values were obtained due to the low electrical conductivity of the GO. However, the combination with MnO_2 led to an increase in the peak current values.

For the CNTs, higher peak current values were observed; however, the addition of MnO_2 increased
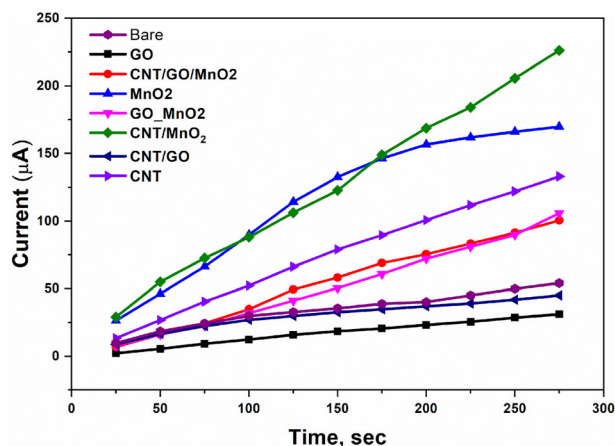
Fig. 10 Chronoamperometric calibration curves of bare, GO, CNTs/GO/MnO_2, MnO_2, GO/MnO_2, CNT/MnO_2, CNT/GO and CNT toward different concentrations of H_2O_2 in PBS pH = 7.4) buffer
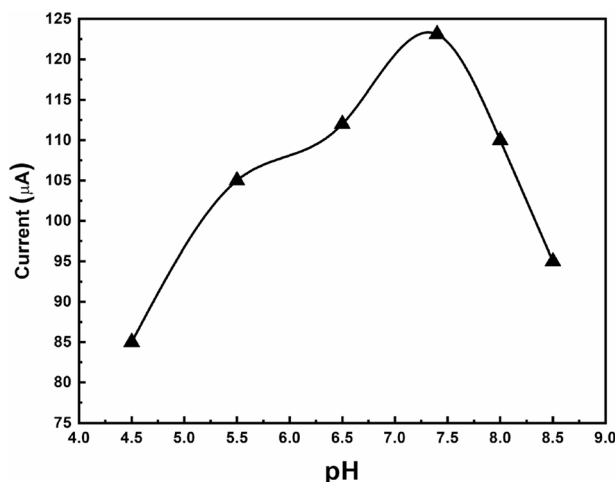
Fig. 11 pH effect on the sensor performance towards the sensitivity of direct peroxides detection

the current values of redox peaks due to its capacitive properties that are assigned to as the MnO_2 characteristics. For the GO/MnO_2/MCNTs, no peak was obtained within the potential range of $-$ 0.38 to 1 V. This is related to the electrical double layer-type behavior; however, a non-Faradaic constant current has been obtained in the entire potential range. However, the cyclic voltammogram exhibited a well-known hysteresis-type loop that is significant for a supercapacitor. Comparison of the specific capacity of GO/MnO_2/MCNTs electrode with the recently reported MnO_2 materials is shown in Table 2.

Worth mentioning here, that all nanomaterials were electrochemically stable over different applied

scan rates, and no damage occurred in the electrode composition as seen in Fig. 9.

## 3.5 The use of MnO_2-based carbon nanocomposite for H_2O_2 detection

The ability to provide high electro-catalytic activity that promotes direct oxidation and fast electron transfer in enzymatic biosensors is one of the key benefits of employing nanocomposite materials as electrode surface modifiers [6]. Thus, the competence of direct electron transfer resulting from the peroxides oxidation was tested among all nanocomposites. In addition, the possibility of direct oxidation was measured after injected different concentrations of peroxides into the electrochemical cell. Figures 10, 11, 12, represent a set of chronoamperometric calibration curves for all modified electrodes, while the higher signals were obtained by electrodes modified with the MnO_2 and MnO_2/CNTs. furthermore, the used nanostructured electrode given the high electro-catalytic activity that enabled the direct electrochemical oxidation of peroxide. Additionally, the oxidation peaks currents were increased as the concentration of H_2O_2 increased which reflect the sensitivity and reliability of the nanostructured modified SPE.

3.5.1 Effect of pH

The chemical composition and the pH of the supporting electrolytes strongly affected electrochemical performance. Thus, effect of the pH changes on the amperometric signal of peroxide oxidation was measured. As illustrated in Fig. 11, the response of the MnO_2/CNTs modified electrode surface towards the oxidation of peroxides was measured at several pHs. As the pH increases from 4.0 up to 7.0, the electrochemical signal increased. However, increasing the pH above 7.5 led to a strong decrease in the peroxide oxidation signal. At this pH, electrode surface modified with the nanomaterial could be protonated, hnce it affected the rate of the electron transfer. So, the pH 7.5 of PBS buffer was selected in all subsequent experiments.

3.5.2 Amperometric deection of peroxide

From the cyclic voltammetry (CV) study, the oxidation peak of peroxide using the modified SPEs with nanocomposites was produced at 0.7 V. Therefore,
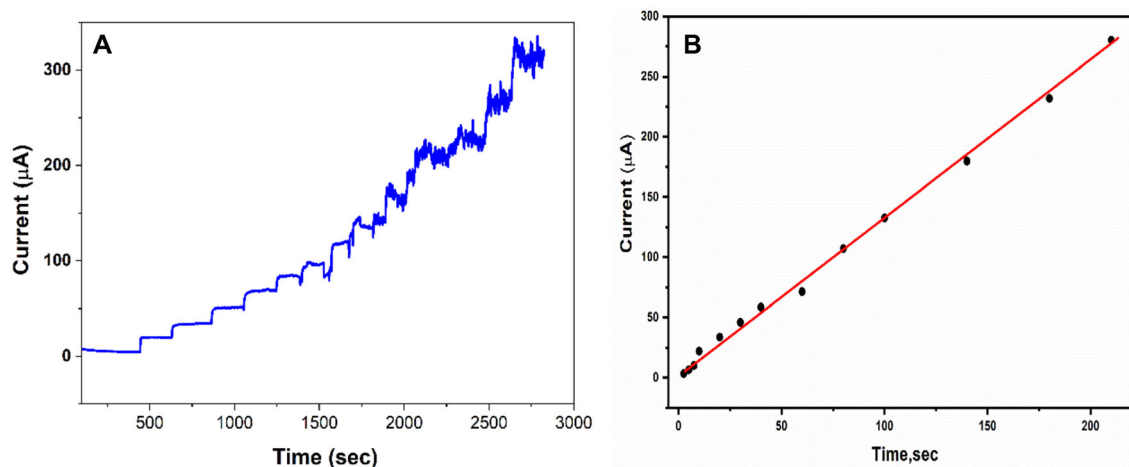
Fig. 12 **A** The corresponding calibration curve toward H_2O_2 response. **B** The corresponding calibration curve toward H_2O_2 response

amperometric detection at 0.7 V was evaluated by standard addition of a certain amount of H_2O_2 at fixed time (30 s).

The relation between current response and the concentration of H_2O_2 (see Fig. 10) showed fast and high response that indicate the fast electron transfer the electro-catalytic behavior of the modified SPE with the selected nanocomposite. Furthermore, the linear range of a calibration curve (as it is clear in Fig. 12A, B) from 1.0 up to 210 μM with the detection limit (S/N = 3) of 0.08 μM approved the high sensitivity of the prepared nanocomposite to be effectively applied for the construction of different enzymatic based biosensors which have important role in biological analysis.

4　Conclusion

In this work, a straightforward, quick, low-temperature, and easy procedure was applied to fabricate various MnO_2-based carbon nanocomposites by a microwave-assisted method. RGO 2D nano-sheets provided a considerable external surface area with outstanding ion adsorption. Notably, the CNTs played a prominent role in the electroactive network and supplied good electrical conductivity and electrolyte accessibility, besides improving the ion diffusion kinetics for additional EDL capacitance. The as-prepared birnessite-MnO_2 provided superior electrochemical performance and high specific capacitance. In addition, the sensing performance of modified electrodes with the nanomaterials has been tested, and the chronoamperometric assay was fully optimized to eventually exploit them for the direct quantitative peroxide concentration. The newly prepared nanocomposites exhibited high supercapacitor efficiency alongside high sensing performance.

Author contributions

All authors contributed to the study conception and design. EO carried out the experiment and collected the data while NY contributed to the data analysis, wrote the manuscript, and designed the figures. The electrochemical, sensor measurement and data analysis were done by HSM, RYAH. EMD were involved in planning and supervised the work. All authors provided critical feedback and helped shape the research, analysis, and manuscript.

Funding

Data availability

Authors confirm that the data supporting the findings of this study are available within the article.

Declarations

Conflict of interest   All authors declare no conflict of interest, whatsoever, with anybody.

References

1. M.S. Guney, Y. Tepe, Classification and assessment of energy storage systems. Renew. Sustain. Energy Rev. **75**, 1187–1197 (2017). https://doi.org/10.1016/j.rser.2016.11.102

2. B.K. Kim, S. Sy, A. Yu, J. Zhang, Electrochemical supercapacitors for energy storage and conversion. Handb. Clean Energy Syst. (2015). https://doi.org/10.1002/9781118991978.hces112

3. Z. Han, Y. Liu, J. Deng, S. Xie, X. Zhao, J. Yang, K. Zhang, H. Dai, Preparation and high catalytic performance of Co_3O_4–MnO_2 for the combustion of o-xylene. Catal. Today (2019). https://doi.org/10.1016/j.cattod.2018.04.042

4. W. Yang, Z. Gao, J. Ma, X. Zhang, J. Wang, Controlled synthesis of Co_3O_4 and Co_3O_4@MnO_2 nanoarchitectures and their electrochemical capacitor application. J. Alloys Compd. **611**, 171–178 (2014). https://doi.org/10.1016/j.jallcom.2014.04.085

5. E.-S. Duraia, S. Niu, G.W. . Beall, Humic acid-derived graphene–SnO_2 nanocomposites for high capacity lithium-ion battery anodes. J. Mater. Sci. Mater. Electron. (2018). https://doi.org/10.1007/s10854-018-8858-x

6. N. Yousf, E. Ouda, H.S. Magar, Y.A. Rabeay, S.A.M. Hassan, E.-S. Duraia, Synthesis, characterization, and electrochemical sensing applications of bimetallic oxide/carbon nanomaterials

hybrids. J. Electrochem. Soc. (2022). https://doi.org/10.1149/1945-7111/ac6458

7. K. Xiao, J.W. Li, G.F. Chen, Z.Q. Liu, N. Li, Y.Z. Su, Amorphous MnO_2 supported on 3D-Ni nanodendrites for large areal capacitance supercapacitors. Electrochim. Acta **149**, 341–348 (2014). https://doi.org/10.1016/j.electacta.2014.10.117

8. C. Julien, A. Mauger, Nanostructured MnO_2 as electrode materials for energy storage. Nanomaterials **7**, 396 (2017). https://doi.org/10.3390/nano7110396

9. J.G. Wang, F. Kang, B. Wei, Engineering of MnO_2-based nanocomposites for high-performance supercapacitors. Prog. Mater. Sci. **74**, 51–124 (2015). https://doi.org/10.1016/j.pmatsci.2015.04.003

10. T. Shinomiya, V. Gupta, N. Miura, Effects of electrochemical-deposition method and microstructure on the capacitive characteristics of nano-sized manganese oxide. Electrochim. Acta. **51**, 4412–4419 (2006). https://doi.org/10.1016/j.electacta.2005.12.025

11. M. Sun, B. Lan, T. Lin, G. Cheng, F. Ye, L. Yu, X. Cheng, X. Zheng, Controlled synthesis of nanostructured manganese oxide: crystalline evolution and catalytic activities. CrystEngComm **15**, 7010–7018 (2013). https://doi.org/10.1039/c3ce40603b

12. H.S. Abd El-Haleem, A. Hefnawy, R.Y.A. Hassan, A.H. Badawi, I.M. El-Sherbiny, Manganese dioxide-core–shell hyperbranched chitosan (MnO_2–HBCs) nano-structured screen printed electrode for enzymatic glucose biosensors. RSC Adv. **6**, 109185–109191 (2016)

13. H.S. Magar, R.Y.A. Hassan, A. Mulchandani, Electrochemical Impedance Spectroscopy (EIS): principles, construction, and biosensing applications. Sensors **21**, 6578 (2021)

14. R.H. Mahmoud, F.A. Samhan, G.H. Ali, M.K. Ibrahim, R.Y.A. Hassan, Assisting the biofilm formation of exoelectrogens using nanostructured microbial fuel cells. J. Electroanal. Chem. **824**, 128–135 (2018)

15. R.H. Mahmoud, F.A. Samhan, M.K. Ibrahim, G.H. Ali, R.Y.A. Hassan, Formation of electroactive biofilms derived by nanostructured anodes surfaces. Bioproc. Biosyst. Eng. **44**(4), 759–768 (2021)

16. A.G. Pandolfo, A.F. Hollenkamp, Carbon properties and their role in supercapacitors. Power Sources **157**, 11–27 (2006). https://doi.org/10.1016/j.jpowsour.2006.02.065

17. Z. Gan, N. Song, H. Zhang, Z. Ma, Y. Wang, C. Chen, One-step electrofabrication of reduced graphene oxide/poly(N-methylthionine) composite film for high performance supercapacitors. J. Electrochem. Soc. (2020). https://doi.org/10.1149/1945-7111/ab8c82

18. Y. Liu, N. Song, Z. Ma, K. Zhou, Z. Gan, Y. Gao, S. Tang, C. Chen, Mater. Chem. Phys. **223**, 548–556 (2019)

19. E. Frackowiak, Carbon materials for supercapacitor application. Phys. Chem. Chem. Phys. **9**, 1774–1785 (2007)

20. Y. Huang, Y. Miao, W.W. Tjiub, T. Liu, High-performance flexible supercapacitors based on mesoporous carbon nanofibers/Co3O4/MnO2 hybrid electrodes. RSC Adv. **5**, 18952–18959 (2015)

21. V. Dhinakaran, B. Stalin, M.S. Sai, J. Vairamuthu, S. Marichamy, Recent developments of graphene composites for energy storage devices. Mater. Today Proc. **45**, 1779–1782 (2021). https://doi.org/10.1016/j.matpr.2020.08.631

22. Q. Zhang, Z. Bai, F. Du, L. Dai, *Carbon nanotube energy applications*, 2nd edn. (Elsevier Inc., Amsterdam, 2019). https://doi.org/10.1016/B978-0-12-812667-7.00028-8

23. H. Jeon, J.M. Jeong, S.B. Hong, M.H. Yang, J. Park, D.H. Kim, S.Y. Hwang, B.G. Choi, Facile and fast microwave-assisted fabrication of activated and porous carbon cloth composites with graphene and MnO2 for flexible asymmetric supercapacitors. Electrochim. Acta. **280**, 9–16 (2018). https://doi.org/10.1016/j.electacta.2018.05.108

24. J. Zhang, H. Zhang, Y. Cai, H. Zhang, Low-temperature microwave-assisted hydrothermal fabrication of RGO/MnO2-CNTs nanoarchitectures and their improved performance in supercapacitors. RSC Adv. **6**, 98010–98017 (2016). https://doi.org/10.1039/c6ra20615h

25. E. Ouda, N. Yousf, M. Morsy, E.M. Duraia, Flexible humidity sensor based on light-scribed graphene oxide. Mater Sci **33**, 18241–18251 (2022). https://doi.org/10.1007/s10854-022-08681-0

26. Y. Sun, K. He, Z. Zhang, A. Zhou, H. Duan, Real-time electrochemical detection of hydrogen peroxide secretion in live cells by Pt nanoparticles decorated graphene–carbon nanotube hybrid paper electrode. Biosens Bioelectron **68**, 358–364 (2015). https://doi.org/10.1016/j.bios.2015.01.017

27. J. Zhang, J. Jianwen, X.S. Zhao, Synthesis and capacitive properties of manganese oxide nanosheets dispersed on functionalized graphene sheets. J. Phys. Chem. C **14**, 6448–6454 (2011)

28. C. Im, Y.S. Yun, B. Kim, H.H. Park, H.J. Jin, Amorphous carbon nanotube/MnO2/graphene oxide ternary composite electrodes for electrochemical capacitors. Nanosci. Nanotechnol. (2013). https://doi.org/10.1166/jnn.2013.6980

29. A.N. Fouda, E.S.M. Duraia, F. El-Tantawy, A facile doping of graphene oxide nanosheets. Rev. Adv. Mater. Sci. **45**, 8–14 (2016)

30. S.N. Alam, N. Sharma, L. Kumar, Synthesis of Graphene Oxide (GO) by modified hummers method and its thermal reduction to obtain Reduced Graphene Oxide (rGO)*. Graphene. **06**, 1–18 (2017). https://doi.org/10.4236/graphene.2017.61001

31. Y. Khan, S.K. Durrani, M. Mehmood, M.R. Khan, Mild hydrothermal synthesis of γ-MnO2 nanostructures and their phase transformation to α-MnO2 nanowires. J. Mater. Res. **26**, 2268–2275 (2011). https://doi.org/10.1557/jmr.2011.138

32. A.N. Fouda, M.A. Assy, G. El Enany, N. Yousf, Enhanced capacitance of thermally reduced hexagonal graphene oxide for high performance supercapacitor carbon nanostructures. Fullerenes Nanotube (2015). https://doi.org/10.1080/1536383X.2014.943889

33. M. Van Tran, A.T. Ha, P.M.L. Le, Nanoflake manganese oxide and nickel-manganese oxide synthesized by electrodeposition for electrochemical capacitor. J. Nanomater. (2015). https://doi.org/10.1155/2015/609273

34. S.M. Husnain, U. Asim, A. Yaqub, F. Shahzad, N. Abbas, Recent trends of MnO2-derived adsorbents for water treatment: a review. New J. Chem. (2020). https://doi.org/10.1039/C9NJ06392G.Volume

35. L. Guan, L. Yu, G.Z. Chen, Capacitive and non-capacitive faradaic charge storage. Electrochim. Acta. **206**, 464–478 (2016). https://doi.org/10.1016/j.electacta.2016.01.213

36. A.A. Ensafi, N. Ahmadi, B. Rezaei, Electrochemical preparation and characterization of a polypyrrole/nickel-cobalt hexacyanoferrate nanocomposite for supercapacitor applications. RSC Adv. **5**, 91448–91456 (2015). https://doi.org/10.1039/c5ra17945a

37. J. Chen, Y. Huang, X. Zhang, X. Chen, C. Li, MnO2 grown in situ on graphene@CNTs as electrode materials for supercapacitors. Ceram. Int. **41**, 12680–12685 (2015). https://doi.org/10.1016/j.ceramint.2015.06.099

38. Z. Lei, F. Shi, L. Lu, Incorporation of MnO 2-coated carbon nanotubes between graphene sheets as supercapacitor electrode. ACS Appl. Mater. Interfaces **4**, 1058–1064 (2012). https://doi.org/10.1021/am2016848

39. Y. Liu, D. He, J. Duan, Y. Wang, S. Li, Synthesis of MnO2/graphene/carbon nanotube nanostructured ternary composite for supercapacitor electrodes with high rate capability. Mater. Chem. Phys. **147**, 141–146 (2014). https://doi.org/10.1016/j.matchemphys.2014.04.020

40. J.L. Yingwen Cheng, Lu. Songtao, H. Zhang, C.V. Varanasi, Synergistic effects from graphene and carbon nanotubes enable flexible and robust electrodes for high-performance supercapacitors. Nano Lett. (2012). https://doi.org/10.1021/nl301804c

41. M. Ramezani, M. Fathi, F. Mahboubi, Facile synthesis of ternary MnO2/graphene nanosheets/carbon nanotubes composites with high rate capability for supercapacitor applications. Electrochim. Acta. **174**, 345–355 (2015). https://doi.org/10.1016/j.electacta.2015.05.155

42. L. Kong, Z. Ren, N. Zheng, S. Du, J. Wu, J. Tang, H. Fu, Interconnected 1D Co3O4 nanowires on reduced graphene oxide for enzymeless H2O2 detection. Nano Res. (2015). https://doi.org/10.1007/s12274-014-0617-6